Design and Operation of Hybrid Microfluidic Iontronic Probes for Regulated Drug Delivery

Theresia Arbring Sjöström, Anton Ivanov, Christophe Bernard, Klas Tybrandt, David Poxson, Daniel Simon, Magnus Berggren

ADVANCED MATERIALS TECHNOLOGIES
www.advmattechnol.de

Design and Operation of Hybrid Microfluidic Iontronic Probes for Regulated Drug Delivery

Theresia Arbring Sjöström, Anton I. Ivanov, Christophe Bernard, Klas Tybrandt, David J. Poxson, Daniel T. Simon, and Magnus Berggren*

Highly controlled drug delivery devices play an increasingly important role in the development of new neuroengineering tools. Stringent—and sometimes contradicting—demands are placed on such devices, ranging from robustness in freestanding devices, to overall device miniaturization, while maintaining precise spatiotemporal control of delivery with high chemical specificity and high on/off ratio. Here, design principles of a hybrid microfluidic iontronic probe that uses flow for long-range pressure-driven transport in combination with an iontronic tip that provides electronically fine-tuned pressure-free delivery are explored. Employing a computational model, the effects of decoupling the drug reservoir by exchanging a large passive reservoir with a smaller microfluidic system are reported. The transition at the microfluidic-iontronic interface is found to require an expanded ion exchange membrane inlet in combination with a constant fluidic flow, to allow a broad range of device operation, including low source concentrations and high delivery currents. Complementary to these findings, the free-standing hybrid probe monitored in real time by an external sensor is demonstrated. From these computational and experimental results, key design principles for iontronic devices are outlined that seek to use the efficient transport enabled by microfluidics, and further, key observations of hybrid microfluidic iontronic probes are explained.

Unravelling fundamental mechanisms and treating neurological disorders including neurodegenerative disease, neural injury, and pain, are both challenging yet very important due to the world-wide burden of these disorders.[1,2] New and highly specific drug delivery tools will facilitate a better understanding of the complex neurobiological environment, and pave the way to highly localized and precise drug delivery technology. To work optimally, such devices need to achieve great chemical and biotarget specificity, while simultaneously limiting biocompatibility issues or pharmaceutical side effects. If these devices are implemented as minimized free-standing probes, they can easily be manipulated to target specific cells or be combined with different experimental setups and sensing technologies to facilitate a wide range of diagnostic and therapeutic capabilities, in particular at deep tissue/organ sites.[3] Here, we compare the capabilities and limitations of two high precision drug delivery techniques, pressure-based microfluidics, and iontronics. In microfluidics, drug transport is highly controlled by regulation of fluidic pressure in miniaturized fluid channels.[4,5] By connecting several fluidic sources and microfabricated fluid channels, mixing, switching, screening, and delivery of various drugs can be easily achieved. The field of microfluidics includes a multitude of experimental setups from lab-on-a-chip devices to free standing microfluidic neural probes.[4,6] The other technique of interest is iontronics, where regulation of applied potentials enables precise dose control and chemical specificity, as long as the drug or neurotransmitter of interest is positively or negatively charged.[7] The most basic iontronic component is the organic electronic ion pump (OEIP). OEIPs are based on a well-defined and encapsulated ion exchange membrane (IEM) separating a source electrolyte reservoir from a target electrolyte (generally referred to as the "ion channel"). Broadly speaking, selectivity of the IEM is dependent on the inherent polarity of the fixed charge, its degree of charge, and its pore size and density. Transport from the source reservoir, through the IEM ion channel, and to the target electrolyte is achieved actively by migration of ions and passive diffusion. By varying an applied potential across the IEM, the migrational ionic delivery rate is controlled electronically and a direct correspondence in applied electronic current and quantity of drug delivered can be established. Planar OEIP devices have been successfully demonstrated for a variety of neurological applications, e.g., by delivery of gamma-aminobutyric acid to suppress epileptiform activity.[8]

T. Arbring Sjöström, Prof. K. Tybrandt, Prof. D. J. Poxson, Prof. D. T. Simon, Prof. M. Berggren
Laboratory of Organic Electronics
Department of Science and Technology
Linköping University
Norrköping 60174, Sweden
E-mail: daniel.simon@liu.se
Dr. A. I. Ivanov, Prof. C. Bernard
Aix Marseille University
INSERM
INS
Inst Neurosci Syst
Marseille 13005, France
The ORCID identification number(s) for the author(s) of this article can be found under https://doi.org/10.1002/admt.202001006.

DOI: 10.1002/admt.202001006

Table 1. Overview of the transport and delivery parameters of pressure-based microfluidic technologies and iontronic device technologies, and how the parameters are inherited upon hybridization.

	Microfluidic devices	Iontronic devices	Hybrid devices
Size of transmitter	Essentially no limit, e.g., drug delivery carriers of several micrometer[4]	Limited to effective pore size, e.g., Indigo carmine[9] (466 g mol^{-1}[13])	Limited to effective pore size
Charge of transmitter	Not required	Required	Required
Main transport mechanism	Pressure	Migration	Pressure and migration
Transport speed	Up to mm s^{-1}[4]	Up to µm s^{-1}[9]	Hybrid transport
Main transport substance(s)	Intended molecule, solvent and other solutes	Intended ion	Intended ion
Delivery mechanism at outlet	Convection and diffusion	Diffusion	Diffusion

Free-standing purely iontronic probe devices are exemplified by capillary OEIPs, where the ion channel is encased in a thin glass capillary.[9]

Comparing pressure-based microfluidics and iontronic drug delivery, several distinctions can be made. Microfluidic systems can deliver any dissolvable drug of virtually any molecular weight[4], while iontronic components are limited to the transport of charged molecules of a relatively limited size/weight range[9]. Further, over extended transport distances microfluidics outperform iontronics since the flow of solute can provide very high flow rates in the range of mm s^{-1}.[4] Comparable transport rates in similar geometry iontronics components are drift velocities in the range of µm s^{-1} (estimated from Ref. [9]). On the other hand, the pressure-free delivery of iontronics is highly desirable for neurological applications since it limits the delivery of secondary substances (solvent, other solutes). Another key advantage to iontronic systems is that while the overall quantity of drug delivered is low, local concentrations at the IEM outlet can be very high since the drug is concentrated by the highly charged IEM itself. In microfluidic delivery, the delivered dose cannot exceed the reservoir concentration and the dissolved ion needs to be delivered together with a volume of its solvent.

A very promising advance in the field of drug delivery is the combination of microfluidic and iontronic methodologies.[10–12] Such hybrid devices can benefit from the advantages of both microfluidics and iontronics while avoiding most of their individual limitations, summarized in **Table 1**. For a successful merger of these technologies into a miniaturized hybrid device, it is of utmost importance to balance the interplay between the hybrid probe's microfluidic chamber and its IEM, by considering several design and operational parameters simultaneously. To investigate how to achieve such a balance, a hybrid microfluidic iontronic probe was designed and investigated theoretically, experimentally realized, and tested. The hybrid probe (**Figure 1**a) presented here uses both microfluidic and electrophoretic transport. Long range microfluidic transport of dissolved drug compounds is performed by inner (feed) and outer (drain) capillary fibers in a coaxial arrangement. In this way, the source electrolyte reservoir is decoupled from the rest of the device. At the hybrid probe's drug delivery tip, the iontronic (electrophoretic) transport is used for short-range highly controlled and fluidic-free delivery into the target system. For convenience, we use the term "transfer chamber" for the region of the device where the fluidic flow interfaces with the IEM and the switch of drug transport mechanism occurs (dashed box in Figure 1a).

The concentration distribution of ions in the transfer chamber, in particular at the surface of the IEM inlet, will have a high impact on how the device responds to applied voltages. For low voltages applied across the IEM, the diffusion of ions from the surrounding electrolyte to the IEM inlet is sufficient to balance the ionic current flow within the IEM. In this ohmic regime, the current response to voltage is linear. With increasing voltages, the concentration at the electrolyte–IEM interface will decrease correspondingly. At sufficiently high voltages, ionic concentration will decrease to form a fully depleted region, where the lack of ions results in a high resistance, locally at the IEM inlet surface. After this point of depletion, the current response to increased voltages reaches a plateau called the limiting current regime.[14,15] Increasing the voltage even further will induce the overlimiting regime, where measured increases in current are largely attributed to electroconvection, and to a lesser degree, water splitting.[14,15] For drug delivery devices, even a small contribution of water splitting to the total current can be problematic since it changes the pH in the electrolyte, reducing dosage control and potentially causing pH changes in the target system. Previous studies have shown that iontronic devices with a miniaturized ion channel inlet suffer from a narrow ohmic regime.[16] In addition to the size of the ion channel inlet, miniaturizing the hybrid probe source reservoir, will further limit the availability of ions in the reservoir. Thus, design and active operational measures must be taken to extend the ohmic regime in order to achieve high and accurate delivery currents in miniatured devices. As such, it has been shown that an extension of the ion channel into the reservoir, referred to as an "ion selective cap" can expand the desired ohmic regime. The ion selective cap increases the effective inlet area and thus provides an increased supply of ions at the ion channel inlet.[16] In other membrane separation processes, it is well known that the overall resistance has a strong dependency on flow rates at the feeding side of the membrane, especially at low concentrations ($<100 \times 10^{-3}$ M).[17] With the hybrid geometry presented here, we investigate if the addition of a constant flow, together with extension of the ion channel into the reservoir, can expand the ohmic regime further.

We investigated the hybrid microfluidic iontronic probe concept with a finite element model based on the Nernst–Planck–Poisson and Navier–Stokes equations using COMSOL Multiphysics software. This computational model was based on both microfluidic capillaries and a cylindrically shaped IEM. An axis-symmetric cylindrical model enabled solutions in 3D geometries by solving a 2D problem.[9,16] We defined the ion channel as an anion exchange membrane (AEM) with 1 M

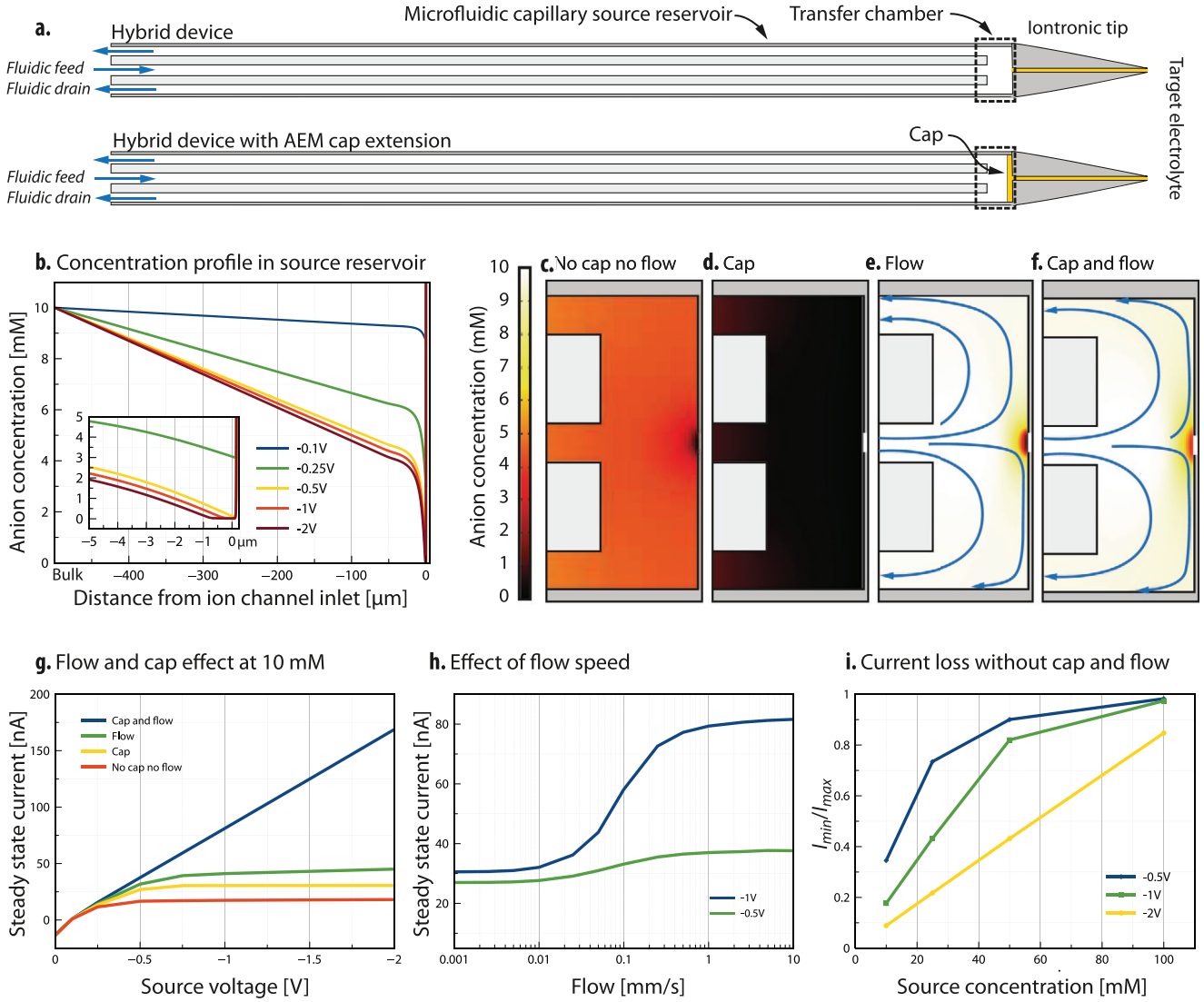

Figure 1. Simulation of flow and ion selective cap effects during operation of the hybrid microfluidic iontronic probe during Glu^- transport. a) Two different versions of the hybrid device are tested, the hybrid device without (top) and with an anion exchange membrane (AEM) cap extension (below). The capillary fluidic system consists of a smaller feed capillary inserted into a larger drain capillary. The encapsulated ion channel responsible for iontronic delivery is connected at the tip of the larger outer capillary. b) Glu^- concentration in the source reservoir at various driving voltages, without flow or ion selective cap. The Glu^- source concentration is fixed to 10×10^{-3} M at the outer boundary (bulk). The inset shows a zoomed view close to the ion channel inlet, highlighting the extension of the ionic depletion zone for increased voltages. Concentration distribution in the transfer chamber with fixed bulk concentration at 10×10^{-3} M, source voltage –1V, can be seen with c) no cap or flow present, d) cap present but without flow, e) no cap but flow, and f) both cap and flow. g) Current–voltage plots show the additional or combinational effect of cap and/or flow at 10×10^{-3} M source concentration. h) Effect of flow rate on steady state current. i) Ratio between the current gained without cap and flow present (I_{min}) compared to the maximum current gained with both (I_{max}) for various voltages.

fixed charge (in line with experimental estimations[9]) and modeled the transport of the excitatory neurotransmitter glutamate (Glu^-) as an exemplar compound for its applicability in neuromodulation. Neuromodulation by Glu^- has the potential to modulate neural information processing by, e.g., altering the spiking activity and modifying long-term synaptic plasticity.[18] More details about the model geometry, simulation parameters and meshing details are found in Figures S1 and S2, Table S1 and S2 (Supporting Information).

First, we used the model to explore device operational characteristics with a non-flow reservoir together with a miniaturized AEM inlet (5 µm radius). The model was simulated at steady state over a voltage range of –0.1 to –2 V with a source concentration of 10×10^{-3} M NaGlu fixed at the fluidic inlet and outlet (bulk), and a target concentration of 160×10^{-3} M NaCl. The concentration profile of Glu^- and Cl^- combined along the *z*-axis of the source reservoir and transfer chamber can be seen in Figure 1b. It can be observed that the concentration in the transfer chamber is characterized as a linear decrease as a function of distance from the bulk, and a more rapid drop near the AEM inlet. From –0.5 V and larger negative potentials, the interface was fully depleted, and the limiting current

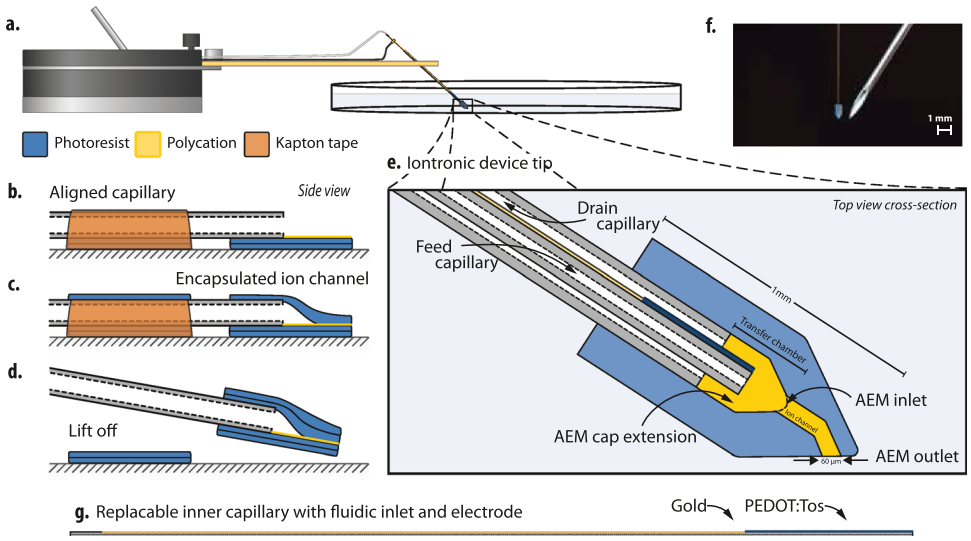

Figure 2. Device and fabrication overview. a) The hybrid microfluidic iontronic probe with a photopatterned iontronic tip in a setup connected to microfluidic and electronic control systems. b) Dry film photoresist enables drop-casting of polymer anion exchange membrane (AEM) and alignment of the 210 µm diameter capillary. The photoresist also c) encapsulates and d) seals the device. e) Cross-section of the device tip shows the fluidic feed and drain as well as the iontronic tip without the sealing lid. f) Photo of the fabricated device in relation to a standard syringe tip. g) The separate feed capillary, with a 90 µm outer diameter, acts as source electrode (PEDOT:Tos) as well as fluidic feed for electrolyte flow and exchange during operation.

regime was reached. At the larger negative voltages, the depletion zone extended further into the electrolyte, as seen in the inset plot. The surface plot in Figure 1c shows the concentration distribution in the transfer chamber for a –1 V bias at 10×10^{-3}. We then used the model to investigate methods to expand the ohmic regime. This was done by introducing two components to the model: i) an AEM cap extension, in this case a 0.5 µm thick and 150 µm wide extension of the AEM into the transfer chamber (Figure 1a), and ii) a constant flow in the source reservoir. These additions to the model were investigated separately and in combination. While the addition of the cap greatly increased the inlet area of the device, nevertheless, this entire extended inlet surface was still depleted during operation, leading to an overall lower concentration in the transfer chamber in the steady state (Figure 1d). Adding only a flow to the transfer chamber (with no cap present) removed the linear drop in concentration but did not remove the depletion zone at the small channel inlet (Figure 1e). The combination of the two methods can be seen in Figure 1f. The linear drop along the channel was removed by the flow, and while the drop at the inlet was still present, full depletion did not occur and the device operated in the (now expanded) ohmic regime. Figure 1g shows the resulting current–voltage responses at 10×10^{-3} M for the four computational models. Note that over-limiting effects were not included in these computations, explaining the constant plateaus. From our models, it is evident that neither fluidic flow nor ion selective cap solutions are individually sufficient to keep the device out of the limiting current regime at a source concentration of 10×10^{-3} M in this voltage/current range. However, combining fluidic flow with the IEM cap shows a significant synergistic effect, making it possible to operate the device in a greatly expanded ohmic regime. As compared to the majority of previously reported OEIPs,[8,9,16] the miniaturized IEM channel of our hybrid probe has a relatively low resistance channel, resulting in relatively high delivery currents at low voltage. To investigate the influence of the microfluidic flow rate on delivery current, the flow rate was gradually increased, and the corresponding steady state delivery current was estimated (Figure 1h). At flow rates above 1 mm s^{-1} we see a clear increase of steady state delivery currents for both –0.5 and –1 V. A flow rate of 5 mm s^{-1} was thus chosen and set as the constant flow rate in all simulations where flow is included. This level is low enough to avoid excessive pressure in the capillary, while high enough to gain the wanted effect. To further estimate how the resulting delivery current is affected by the operational conditions, simulations were performed over a concentration range of 10 to 100×10^{-3} and for a voltage range of –0.5 to –2 V, with and without including the cap and the flow. Figure 1i shows the ratio of how much the limited minimum current (I_{min}) in fact is limited with neither cap nor flow implemented, compared to the maximum current ($I_{max} = 1$) achieved with both cap and flow present. As expected, these results show that the combined effects of cap and flow are less pronounced at higher concentrations.

As a complement to our simulation studies, we developed a fabrication protocol for a hybrid microfluidic iontronic probe (**Figure 2**) following the design principles from the modeling above. The iontronic component at the tip of the capillary was fabricated, encapsulated, and sealed by repeated steps of lamination and UV patterning of a dry film photoresist (DFP, Ordyl SY355 (Elga Europe)), drop casting of the AEM (hyperbranched polyglycerol (HPG) functionalized with positive terminal groups (C-HPG)[9,19,20]), and placement of the capillary fiber (Figure 2b–d). Details about the fabrication protocol can be found in Figure S3 (Supporting Information). By extending the AEM into the transfer chamber by drop casting the entire surface with C-HPG, a version of the cap was achieved. The resulting outer dimensions of the iontronic component (blue in

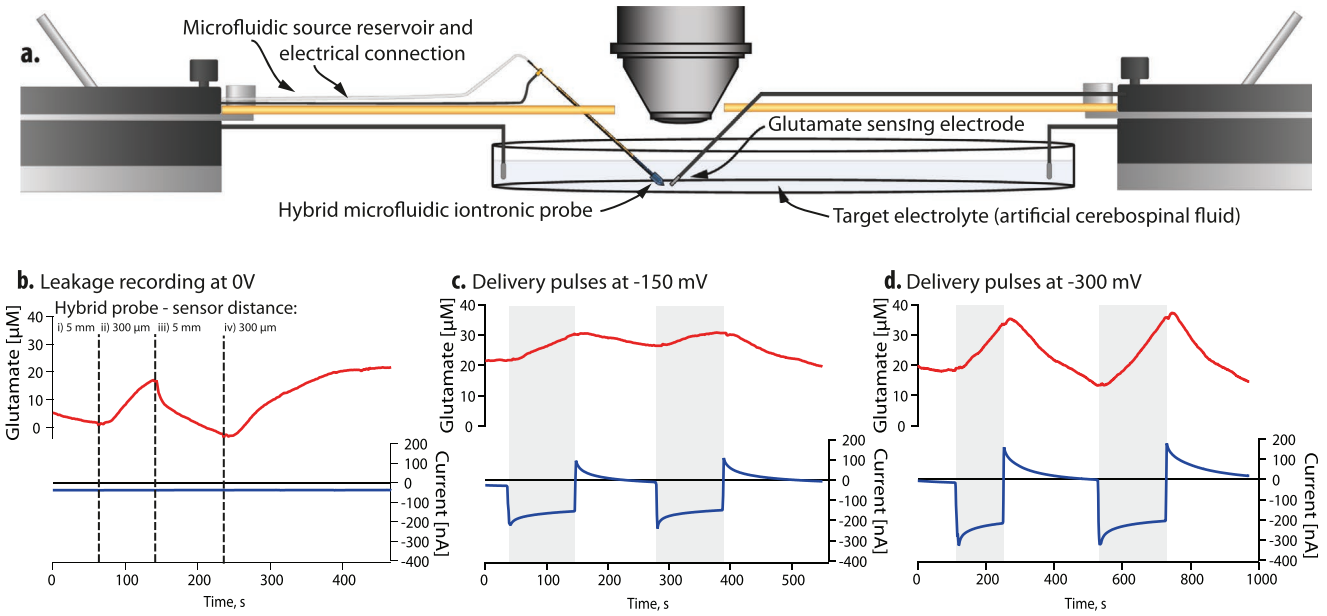

Figure 3. Device characterization of Glu^- delivery. a) The free-standing hybrid microfluidic iontronic probe and Glu^- sensing electrode enables real-time delivery characterization. b) Passive delivery (red trace) at 0 V measured at distances i) 5 mm, ii) 300 µm, iii) 5 mm, and iv) 300 µm from the hybrid probe outlet. Dashed lines indicate movement of the sensor. Active delivery (red trace) measured during voltage pulses (light gray intervals) of c) −150 mV and d) −300 mV bias.

Figure 2e,f) were 650 µm wide by 1 mm long. At this size, effective sealing around the outer capillary, as well as, around the AEM was achieved, even under pressure from the microfluidic control syringe pump for a majority of the fabricated devices. Essentially, the hybrid probe must be connected to the electronic control systems, via the capillaries. Electric conduction in small electrolyte capillaries creates a large electrical resistance that can easily exceed the resistance of the ion channel, causing the applied potential to drop over the electrolyte capillary rather than across the ion channel. To bypass the high electrical resistance in the microfluidic capillary, the source electrode needs to be brought close to the ion channel inlet. We solved this issue by electropolymerizing a PEDOT:Tos electrode[21] on the outside of the inner feed capillary, close to its tip (Figure 2g). This arrangement also enables the source electrode to be replaced as needed, extending the life of the hybrid probe. Thus, the finalized hybrid probe comprises two separate parts: (i) the outer drain capillary plus iontronic tip, and (ii) the replaceable inner feed capillary with connections to the microfluidic and electronic control systems. This enables precise placement of the iontronic delivery tip at the target of interest, with the inner feed and control systems incorporated only during active operation. The stiffness of the glass capillary and DFP material lends itself to probe applications in vitro. However, the overall device tip geometry remains large in terms of many in vivo biological applications, thus, this specific device geometry may not be a suitable alternative for insertion into tissue.

The fabricated hybrid probe was characterized during simultaneous fluidic and electrical biasing operation. Evaluating the active delivery—and passive delivery—characteristics of local and low dose delivery devices is generally challenging since many sensing techniques suffer from a high limit of detection.[22] Here, an enzymatic/amperometric Glu^- sensing electrode (Sarissa Biomedical, UK) was used for local, highly sensitive, and real-time characterization of passive and active delivery of Glu^- (**Figure 3**). When the Glu^- electrode sensing tip was positioned 5 mm away from the hybrid probe tip (i), a low amplitude sensing current was measured that we attribute to either intrinsic sensor noise or low concentrations of Glu^- passively leaking from the probe (Figure 3b, red trace). The Glu^- concentration increased when the sensor was moved to a 300 µm distance from the hybrid probe (ii) and decreased when the sensor was withdrawn (iii). After a second time approaching the hybrid probe outlet, a steady state value of approximately 22×10^{-3} M was measured (iv). The active delivery was tested at −150 mV and measured as a 0.09×10^{-6} M s^{-1} increase in Glu^- concentration (Figure 3c, red trace). A −300 mV potential increased the Glu^- delivery rate to 0.12×10^{-6} M s^{-1} (Figure 3d, red trace). The concentration levels and the timing of concentration variations measured in this setup depend on the distance between the delivery tip and the sensor, the actual delivery rate of Glu^- from the device, and the response time of the sensor. From experience with the same Glu^- sensor, we assume a low contribution of the sensor response time (<500 ms [23]) and thus only a minor averaging effect during transient measurements. In both cases, after switching back to 0 V, the Glu^- concentration decreased to the initial level. To achieve a higher on/off (active flux/passive flux) with a resistor-type component, the ion channel resistance and following driving voltage needs to be higher.[24] A straightforward way of achieving a higher ion channel resistance is to reduce the cross-section of the IEM.

Here, a hybrid microfluidic and iontronic drug delivery system is experimentally realized, where simultaneous utilization of fluid flow and electrophoretic transport is demonstrated and scrutinized. Theoretical investigation of the transition from microfluidic to iontronic transport in the transfer chamber, and

its impact on device performance, was also performed using a computational model. The model indicates that in miniaturized hybrid devices, the synergistic effect of an extended ion channel into the inlet area in combination with a constant fluidic flow can assure a broad window of operation, i.e., low source concentrations and/or high delivery currents. However, one can easily drive these hybrid devices into the limiting and over-limiting regime by applying only marginally higher voltages. Therefore, computational models with estimations of a specific design and experiment parameters are highly valuable for defining a hybrid probe's operational window and ensuring optimal performance. Our experiments also show that if the iontronic component at the probe's delivery tip is based on a resistor type component with a low built-in resistance, diffusional delivery in the passive "off" state needs careful consideration. The passive delivery could also be alleviated using the microfluidic system, since it could be used not only for providing or switching between drug solution, but also to exchange the drug solution for a buffer solution. In this way, passive delivery between the delivered doses can be prevented without any active reversed biasing of the iontronics, thereby simplifying the control circuitry. However, if the application requires minimal passive delivery, the iontronic component could incorporate an ionic diode.[25,26] In summary, the device here demonstrated illuminates key considerations for future free-standing hybrid delivery probes, capable of a broad range of applications. The iontronic tip can be expanded into a more complex "delivery chip" with several control electrodes and vertical delivery outlets.[26,27] And regardless of the device tip design, such devices will all benefit from the decoupled and replaceable inner electrode capillary and the powerful and versatile microfluidic source reservoir.

Experimental Section

Simulations were performed using finite element modeling in COMSOL Multiphysics 5.5 using Tertiary current distribution and Creeping flow physics interfaces. A model overview (Figure S1, Supporting Information), parameter list (Tables S1 and S2, Supporting Information), and meshing details (Figure S2, Supporting Information), as well as the fabrication protocol of the iontronic tip (Figure S3, Supporting Information) are detailed in the Supporting Information. The fabricated device was filled in with 75×10^{-3} M of NaGlu (aqueous) and connected to a syringe pump (Pilot1, made by Fresenius Kabi, Germany) containing the same solution. The target solution was artificial cerebrospinal fluid (2 mL) not containing Glu^-. An SBS-Glu-05-25 enzymatic amperometric Glu^- sensing electrode (Sarissa Biomedical, UK) was used to detect concentration changes. The slight drift from the baseline of the Glu^- signal observed in the beginning of the recording is a result of the slow decrease in the temperature of the target solution. No temperature control equipment was used to avoid convection flows that would perturb the passive diffusion of Glu^-. Both the hybrid probe and the Glu^- sensing electrode was driven by two channel picoammeter PA2000 (Unisense, Danmark). Silver chloride pellets were used as reference electrodes. The Glu^- sensing electrode was kept at +0.5 V in all experiments.

Supporting Information

Supporting Information is available from the Wiley Online Library or from the author.

Acknowledgements

The authors wish to thank Kosala Wijeratne for the electropolymerization of PEDOT:Tos, and Tobias Abrahamsson for providing C-HPG. Mikhail Vagin, and Erik Gabrielsson for their input and critical discussion, and Henrik Ekström for his assistance with COMSOL. This work was funded by grants from the Swedish Foundation for Strategic Research, the Knut and Alice Wallenberg Foundation, Vinnova, and the FLAG-ERA JTC2017 project EPIGRAPH (ANR-17-GRF2-0001). Additional funding was provided by the Swedish Research Council, the European Research Council (ERC Advanced Grant 2018, Magnus Berggren), the Swedish Government Strategic Research Area in Materials Science on Advanced Functional Materials at Linköping University (Faculty Grant SFO-Mat-LiU No. 2009-00971) and A*MIDEX ION project 2IONXXID/REID/ID17HRU208.

Conflict of Interest

The authors declare no conflict of interest.

Keywords

bioelectronics, drug delivery, iontronics, microfluidics, organic electronics

Received: October 10, 2020
Revised: November 19, 2020
Published online: January 14, 2021

[1] V. L. Feigin, T. Vos, N. D. C. Group, *Lancet Neurol.* **2017**, *16*, P877.
[2] D. Borsook, *Brain* **2012**, *135*, 320.
[3] D. A. LaVan, T. McGuire, R. Langer, *Nat. Biotechnol.* **2003**, *21*, 1184.
[4] H. A. Santos, D. Liu, H. Zhang, *Microfluidics for Pharmaceutical Applications: From Nano/Micro Systems Fabrication to Controlled Drug Delivery*, Elsevier, NY **2019**.
[5] N. Convery, N. Gadegaard, *Micro Nano Eng.* **2019**, *2*, 76.
[6] J. Y. Sim, M. P. Haney, S. Il Park, J. G. Mccall, J.-W. Jeong, *Lab Chip* **2017**, *17*, 1406.
[7] T. Arbring Sjöström, M. Berggren, E. O. Gabrielsson, P. Janson, D. J. Poxson, M. Seitanidou, D. T. Simon, *Adv. Mater. Technol.* **2018**, *3*, 1700360.
[8] A. Williamson, J. Rivnay, L. Kergoat, A. Jonsson, S. Inal, I. Uguz, M. Ferro, A. Ivanov, T. A. Sjöström, D. T. Simon, M. Berggren, G. G. Malliaras, C. Bernard, *Adv. Mater.* **2015**, *27*, 3138.
[9] D. J. Poxson, E. O. Gabrielsson, A. Bonisoli, U. Linderhed, T. Abrahamsson, I. Matthiesen, K. Tybrandt, M. Berggren, D. T. Simon, *ACS Appl. Mater. Interfaces* **2019**, *11*, 14200.
[10] C. M. Proctor, A. Slézia, A. Kaszas, A. Ghestem, I. del Agua, A.-M. Pappa, C. Bernard, A. Williamson, G. G. Malliaras, *Sci. Adv.* **2018**, *4*, eaau1291.
[11] C. M. Proctor, I. Uguz, A. Slezia, V. Curto, S. Inal, A. Williamson, G. G. Malliaras, *Adv. Biosyst.* **2019**, *3*, 1800270.
[12] S.-T. Chen, C. M. Proctor, G. G. Malliaras, *Sci. Rep.* **2020**, *10*, 7185.
[13] National Center for Biotechnology Information, "Indigo carmine ($C_{16}H_8N_2Na_2O_8S_2$), http://pubchem.ncbi.nlm.nih.gov/compound/Indigo-carmine#section=Computed-Properties, n.d.
[14] J. J. Krol, M. Wessling, H. Strathmann, *J. Membr. Sci.* **1999**, *162*, 145.
[15] V. V. Nikonenko, A. V. Kovalenko, M. K. Urtenov, N. D. Pismenskaya, J. Han, P. Sistat, G. Pourcelly, *Desalination* **2014**, *342*, 85.
[16] M. Seitanidou, K. Tybrandt, M. Berggren, D. T. Simon, *Lab Chip* **2019**, *19*, 1427.
[17] P. Długołecki, P. Ogonowski, S. J. Metz, M. Saakes, K. Nijmeijer, M. Wessling, *J. Membr. Sci.* **2010**, *349*, 369.

[18] L. M. Giocomo, M. E. Hasselmo, *Mol. Neurobiol.* **2007**, *36*, 184.
[19] D. J. Poxson, M. Karady, R. Gabrielsson, A. Y. Alkattan, A. Gustavsson, S. M. Doyle, S. Robert, K. Ljung, M. Grebe, D. T. Simon, M. Berggren, *Proc. Natl. Acad. Sci. USA* **2017**, *114*, 4597.
[20] T. Abrahamsson, D. J. Poxson, E. O. Gabrielsson, M. Sandberg, D. T. Simon, M. Berggren, *Front. Chem.* **2019**, *7*, 484.
[21] K. Wijeratne, M. Vagin, R. Brooke, X. Crispin, *J. Mater. Chem. A* **2017**, *5*, 19619.
[22] S. D. Niyonambaza, P. Kumar, P. Xing, J. Mathault, P. De Koninck, E. Boisselier, M. Boukadoum, A. Miled, *Appl. Sci.* **2019**, *9*, 4719.
[23] A. Malkov, A. I. Ivanov, A. Latyshkova, P. Bregestovski, M. Zilberter, Y. Zilberter, *Ann. Neurol.* **2019**, *85*, 907.
[24] K. Tybrandt, K. C. Larsson, S. Kurup, D. T. Simon, P. Kjäll, J. Isaksson, M. Sandberg, E. W. H. Jager, A. Richter-Dahlfors, M. Berggren, *Adv. Mater.* **2009**, *21*, 4442.
[25] E. O. Gabrielsson, M. Berggren, *Biomicrofluidics* **2013**, *7*, 064117.
[26] A. Jonsson, T. Arbring Sjöström, K. Tybrandt, M. Berggren, D. T. Simon, *Sci. Adv.* **2016**, *2*, e1601340.
[27] T. Arbring Sjöström, A. Jonsson, E. O. Gabrielsson, M. Berggren, D. T. Simon, K. Tybrandt, *Adv. Mater. Technol.* **2020**, *5*, 1900750.